

# Confocal Micro-PL Mapping of Defects in CdTe Epilayers Grown on Si (211) Substrates with Different Annealing Cycles

HENAN LIU,<sup>1</sup> YONG ZHANG,<sup>1,3</sup> YUANPING CHEN,<sup>2</sup>  
and PRIYALAL S. WIJEWARNASURIYA<sup>2</sup>

1.—University of North Carolina at Charlotte, Charlotte, NC, USA. 2.—US Army Research Laboratory, Adelphi, MD, USA. 3.—e-mail: yong.zhang@uncc.edu

We have applied confocal microphotoluminescence ( $\mu$ -PL) microscopy to investigate the effects of extended defects in CdTe epilayers grown on (211) Si substrates with different numbers of annealing cycles  $N$ . Our results show that the PL dark spot density (PL-DSD) decreases while the spatially averaged PL intensity increases with increasing number of annealing cycles. This is consistent with the general trend that an increase in the number of annealing cycles leads to a reduction of the x-ray diffraction linewidth and etch pit density (EPD). However, direct comparison between the etch pits, imaged by scanning electron microscopy, and PL dark spots on the same sample area results in two important observations: (1) the PL-DSD is substantially higher than the EPD, and (2) not all etch pits appear as dark spots in PL maps. These findings suggest that PL mapping is a more sensitive technique for revealing the extended defects that are actually detrimental to photogenerated carriers, in addition to the apparent advantages of being noninvasive and more efficient.

**Key words:** CdTe,  $\mu$ -PL, defects, EPD

## INTRODUCTION

CdTe is an important semiconductor material currently used in a number of applications, such as infrared (IR) detection, the photovoltaics (PV) industry, and x-ray and gamma-ray detection.<sup>1</sup> Besides, due to the relatively small lattice mismatch, it serves as the buffer layer in HgCdTe epitaxial growth. Extended defects in a semiconductor, such as dislocations, will drastically deplete the photogenerated carriers near the defects through nonradiative recombination,<sup>2</sup> which consequently impacts device performance. When CdTe is serving as a buffer layer, its extended defects will affect the epitaxial growth, and consequently influence the epilayer's quality, as in the case of HgCdTe grown on CdTe.<sup>3</sup> Therefore, study and analysis of extended defects in CdTe epilayers can aid in understanding and evaluating material quality.

Photoluminescence (PL) has long been used as an effective and noninvasive method to study defects in CdTe.<sup>4-6</sup> The conventional, macro-PL technique can only provide the PL intensity averaged over a macroscopic region that might contain many different kinds of defect. The confocal micro-PL ( $\mu$ -PL) technique, on the other hand, ensures that the collected PL signals originate from a well-defined volume of submicron scale at the excitation site;<sup>7</sup> hence, it offers superior spatial resolution compared with the macro-PL technique.<sup>8</sup> This high spatial resolution enables study of the distribution of defects and corresponding statistical analyses. In this work, we performed confocal  $\mu$ -PL mapping on a set of CdTe epilayers grown on Si (211) substrates, intending to investigate the effects of extended defects, presumably dislocations. These epilayers differ in terms of the number of annealing cycles applied.<sup>3</sup> The results are correlated with those from other characterization methods, such as x-ray diffraction (XRD) linewidth, and the etch pit density (EPD) found by chemical etching. Notably, we attempted to compare the PL dark spot density

(Received October 21, 2013; accepted March 14, 2014;  
published online April 18, 2014)

(PL-DSD) with the EPD. To explore the correlation between the PL dark spots and etch pits, we compared the PL dark spots and etch pits on the same area by firstly performing PL mapping, then chemical etching, and finally scanning electron microscopy (SEM) imaging.

### EXPERIMENTAL PROCEDURES

A Horiba HR 800 confocal Raman microscope (Horiba Jobin-Yvon Inc., Edison, NJ) was used for PL mapping acquisition, with measurements conducted at room temperature. A 532-nm laser was used as the excitation source, with power of 0.3 mW. The diffraction-limited laser spot size was approximately  $0.72 \mu\text{m}$  through a  $100\times$  objective lens (numerical aperture 0.9), and the spatial resolution was about half of the laser spot size ( $0.36 \mu\text{m}$ ). The PL signals were captured by a charge-coupled device (CCD) detector (Horiba Jobin-Yvon Inc., Edison, NJ). The PL mapping concerned the feature centered at 822 nm, which corresponds to the excitonic emission of CdTe at room temperature.<sup>9</sup> The signals were collected from a 22-nm bandwidth. For each of the epilayers, the mapping area was  $20 \mu\text{m} \times 20 \mu\text{m}$ , with step size of  $0.5 \mu\text{m}$ . These examined areas were carefully chosen so that they were free of surface defects. A total of six epilayers were examined, differing in the number of annealing cycles  $N$ . Details regarding material growth can be found in a previous publication.<sup>3</sup> The EPD and XRD linewidth were obtained beforehand, on a separated piece of the sample cut from that used for PL mapping. Furthermore, to correlate the PL dark spots to structural defects, such as dislocations, we selected the epilayer with  $N = 8$  annealing cycles to make a direct comparison between PL dark spots and etch pits in the same area. After PL mapping, it was chemically etched using conventional Everson etching to reveal the etch pits.<sup>10</sup> The etch pits were observed under a high-magnification optical microscope, and more clearly by SEM. The SEM image was obtained by using a Raith 150 E-beam lithography system (Raith USA Inc., Islip, NY). The accelerating voltage was 10 kV, the aperture size was  $30 \mu\text{m}$ , and the magnification was 2480. A laser was used to generate markers on this epilayer so that we could identify the area after etching, which

ensured that the subsequent comparisons between PL and SEM were reliable.

### RESULTS AND DISCUSSION

Figure 1 summarizes the PL mapping data for the six samples with  $N = 0, 2, 4, 6, 8,$  and  $10$  annealing cycles. In general, a large number of PL dark spots were resolved, corresponding to sites of low PL intensity. These dark spots were likely to be associated with extended defects, and the PL-DSD varied from sample to sample. A general trend was clearly observed: the PL-DSD reduced with increasing number of annealing cycles, with an optimal value of  $N_{\text{op-PL}} = 8$ . This observation is generally consistent with the reduction in the EPD and XRD linewidth observed with increasing number of annealing cycles,<sup>3</sup> although the optimal annealing cycle number was different for different measurements, namely  $N_{\text{op-XRD}} = 6$  and  $N_{\text{op-EPD}} = 10$  (Table I).

Figure 2 shows representative optical images of these six samples after etching, under a  $100\times$  objective lens. The etch pits are the triangular-shaped pits in this figure. When considering the density levels, there is very good qualitative correspondence between the PL dark spots and the etch pits resolved in the optical images; For instance, the  $N = 0$  epilayer has the largest PL-DSD, and its EPD in the optical image is also the largest. Meanwhile, the  $N = 8$  epilayer has the lowest PL-DSD, and its EPD is also the lowest. Besides, this epilayer also has the smoothest surface after etching. Unfortunately, the sample areas shown in Fig. 1 do not correspond to those shown in Fig. 2, thus no direct comparison can be made.

Figure 3 shows histogram plots of the PL mapping data from Fig. 1, providing clear statistical insight into the PL results and allowing a more quantitative discussion. The PL-DSDs and normalized averaged PL intensities for all the samples are summarized in Table I. These results are consistent with the observed trend between the EPD and number of annealing cycles: the EPD decreases with increasing  $N$ . The PL mapping data also show a similar trend: the PL-DSD decreases with increasing  $N$  (except for  $N = 10$ ). Quantitatively, however, the PL-DSD seems to be somewhat higher than the corresponding EPD for the same sample; For

**Table I. Summary of characterization results of CdTe epilayers grown on Si (211) substrates**

Sample	Thickness ( $\mu\text{m}$ )	Growth Temperature ( $^{\circ}\text{C}$ )	XRD FWHM (arcsec)	Annealing Cycles, $N$	EPD ( $10^7 \text{ cm}^{-2}$ )	PL-DSD ( $10^7 \text{ cm}^{-2}$ )	Averaged PL Intensity (Normalized)
32207	8.95	280.0	110	0	2.7	5.6	0.527
32707	8.8	280.0	86	2	1.6	3.95	0.964
40307	9	280.0	79	4	0.98	3.65	0.753
32807	8.8	280.0	56	6	0.13	2.675	0.799
32607	8.9	280.0	61	8	0.077	2.325	1.000
32307	8.8	280.0	58	10	0.043	3.375	0.911

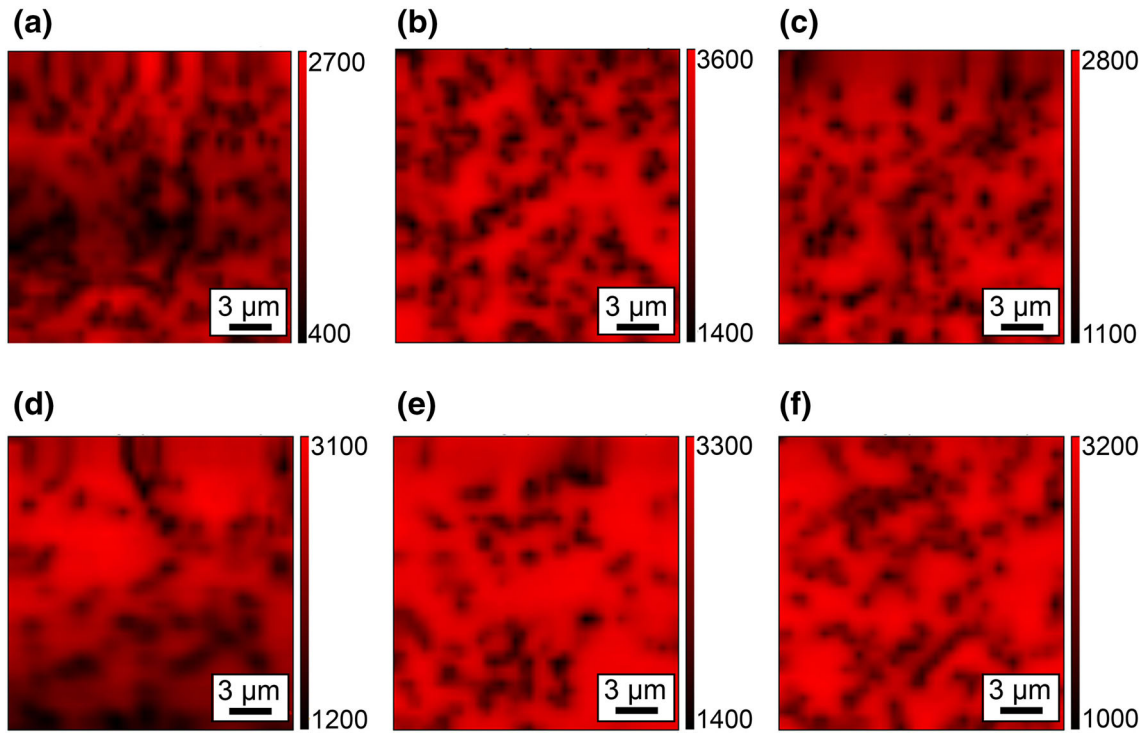


Fig. 1. PL intensity maps of CdTe epilayers with different numbers of annealing cycles  $N$ : (a)  $N = 0$ , (b)  $N = 2$ , (c)  $N = 4$ , (d)  $N = 6$ , (e)  $N = 8$ , and (f)  $N = 10$ ; the area is  $20 \mu\text{m} \times 20 \mu\text{m}$ .

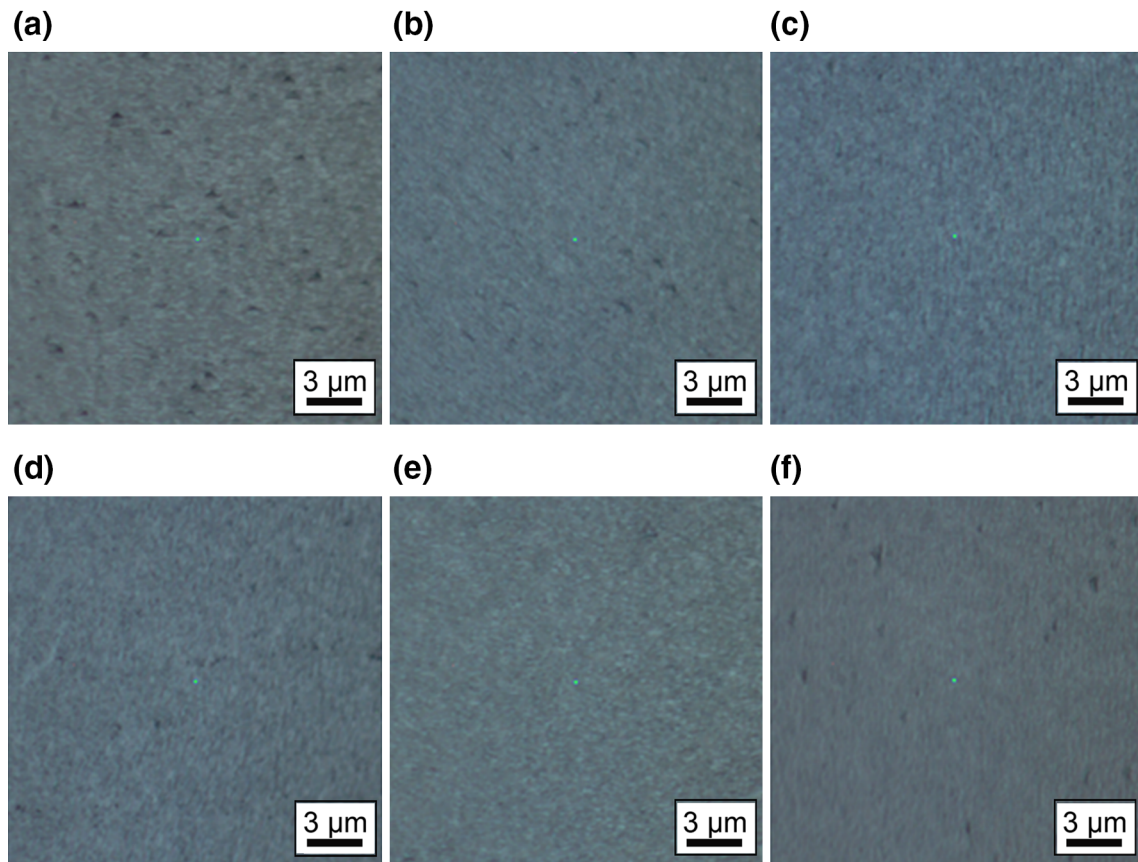


Fig. 2. Optical images of samples with different  $N$  values: (a)  $N = 0$ , (b)  $N = 2$ , (c)  $N = 4$ , (d)  $N = 6$ , (e)  $N = 8$ , and (f)  $N = 10$ .

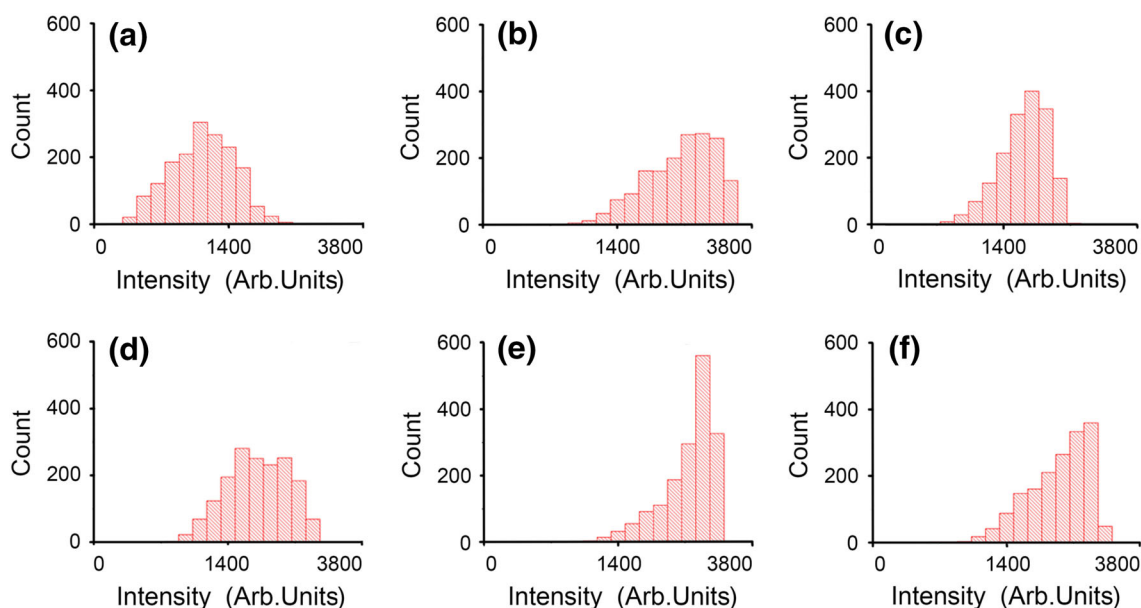


Fig. 3. Histogram plots of the PL mapping data shown in Fig. 1 for: (a)  $N = 0$ , (b)  $N = 2$ , (c)  $N = 4$ , (d)  $N = 6$ , (e)  $N = 8$ , and (f)  $N = 10$ ; note that the axis ranges are the same for all plots.

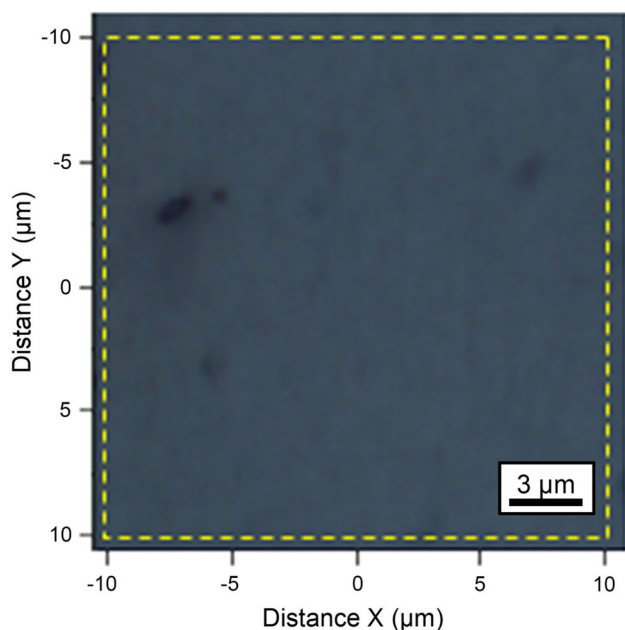


Fig. 4. Optical image (under 100 $\times$  objective lens) for sample 32607.

instance, the former is  $\sim 20$  times as large as the latter for the  $N = 8$  epilayer. This discrepancy could be due to the sensitivity difference between the two techniques, but may also be related to the fact that the EPD and PL-DSD were not measured from exactly the same area. The spatially averaged PL intensity increases with increasing number of annealing cycles, reaching a maximum at  $N = 8$ , for which the PL-DSD was found to be the lowest. However, this averaged PL intensity does not

necessarily follow a simple monotonic dependence on  $N$ . In addition, it is worth noting that, among the six samples, the  $N = 8$  epilayer showed not only the highest averaged PL intensity but also the sharpest distribution in the histogram plot; That is, there were more test points showing high-intensity PL signals than for the other five samples.

To further examine the possible correlation between the PL dark spots and the etch pits, we needed to compare them in exactly the same area. To achieve this goal, we identified (with appropriate laser markers) a  $20 \mu\text{m} \times 20 \mu\text{m}$  area free of any apparent surface defects, on sample #32607 ( $N = 8$ ). The optical image of this area after chemical etching is shown in Fig. 4. The PL mapping result is shown in Fig. 5a, and the SEM image after etching is shown in Fig. 5b. The darker regions near the center and at the lower left corner of the SEM image were due to unintended electron beam damage. Through comparison of these two results, we unambiguously confirmed that the PL-DSD is substantially higher than the EPD, as found previously on the same sample but not the same area. The 12 etch pits counted in the SEM image within the PL mapping area yield an EPD of  $\sim 0.3 \times 10^7 \text{ cm}^{-2}$ , which is somewhat higher than the value given in Table I (obtained from an optical image and thus with lower resolution). The PL-DSD from the same area is  $\sim 2.1 \times 10^7 \text{ cm}^{-2}$ , which is much larger than the EPD. More significantly, comparing Fig. 5a with Fig. 5b, three scenarios are observed: (1) There is a clear match between an etch pit and a PL dark spot. Solid circles in both Fig. 5a and b indicate the etch pits matched to PL dark spots at the same locations (within the accuracy of the PL scan). (2) Etch pits cannot be clearly matched to any PL dark spot, even

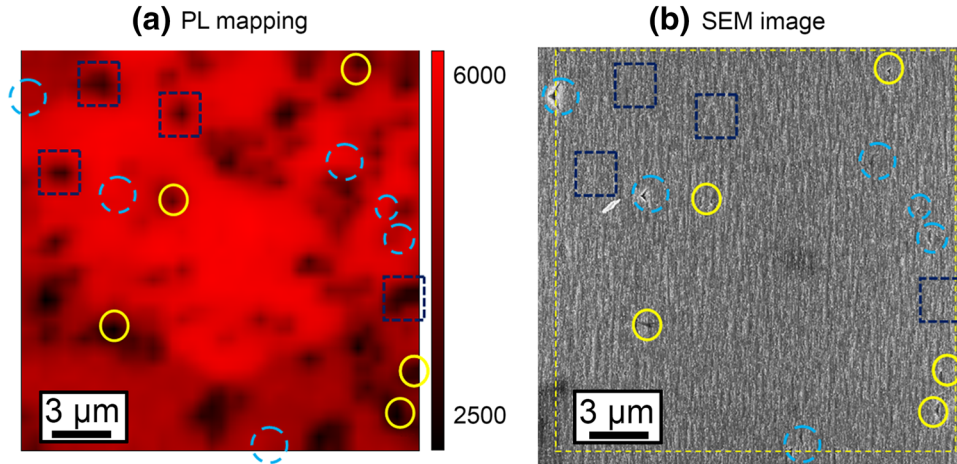


Fig. 5. Comparison of PL intensity mapping (before etching) with SEM image (after etching) for sample 32607 ( $N = 8$ ) for the same area of Fig. 4.

though the overall PL-DSD is significantly higher than the EPD. Dotted circles indicate such etch pits. The fact that a number of etch pits cannot be correlated to appropriate PL dark spots suggests that not all defects are equally detrimental to photo-generated carriers. In fact, some could even be benign. (3) PL dark spots do not show as etch pits: a number of PL dark spots were resolved at locations that are free of etch pits. We indicate only some of these PL dark spots using dotted squares. This finding suggests that the PL mapping offers higher sensitivity than chemical etching for identifying those defects harmful to photogenerated carriers, although it may not be able to reveal all dislocation-type defects, assuming that all the etch pits originate from dislocations. One possibility could be that there are other types of defect that can manifest themselves in PL maps as dark spots. Apparently more work is required to understand the implications of the results from the two different measurements. Other techniques will be helpful, such as structural characterization of an individual defect, micro-Raman, and laser beam induced current (LBIC) measurements. However, PL, as a result of carrier radiative recombination, provides a more direct indication of the sample quality relevant to device performance compared with EPD, which merely reflects the structural quality.

This work shows that  $\mu$ -PL mapping in conjunction with statistical analysis provides an effective and nondestructive method to evaluate the extended defect density in a semiconductor epilayer, CdTe in particular. We could further correlate the  $\mu$ -PL mapping data to other characterizations, such as reflectance, Raman, electroluminescence (EL), LBIC, and SEM, to offer more comprehensive understanding of the material. Currently, a theoretical model is being developed to extract the carrier diffusion from the PL mapping data with the presence of multiple defects in a given area, when the defect density is relatively low.

## CONCLUSIONS

We used confocal  $\mu$ -PL microscopy to study extended defects in CdTe epilayers grown on Si (211) substrates with different numbers of annealing cycles. In general, the PL mapping results follow similar trends to the EPD and XRD linewidth. However, direct comparison between the etch pits (imaged by SEM) and PL dark spots on the same sample area showed that: (1) the PL-DSD is substantially higher than the EPD, (2) not all etch pits appear as dark spots in PL maps, and (3) some defects, although not shown as etch pits, also give rise to PL dark spots. These findings suggest that PL mapping is a more sensitive technique for revealing the extended defects that are actually detrimental to photogenerated carriers, in addition to the more apparent advantages of being noninvasive and more efficient. The optimal number of annealing cycles  $N$  was found to be  $N_{\text{op-PL}} = 8$ , yielding the lowest PL-DSD and largest average PL intensity, which is somewhat different from those found using other metrics, i.e.,  $N_{\text{op-XRD}} = 6$  and  $N_{\text{op-EPD}} = 10$ .

## ACKNOWLEDGEMENTS

This project was supported by DARPA/MTO under Contract # W911NF-11-2-0070, which was monitored by Dr. Nibir Dhar. Yong Zhang acknowledges the support of the Bissell Distinguished Professorship.

## REFERENCES

1. R.N. Bicknell, R.W. Yanka, N.C. Giles, J.F. Schetzina, T.J. Magee, C. Leung, and H. Kawayoshi, *Appl. Phys. Lett.* 44, 313 (1984).
2. T.H. Gfroerer, Y. Zhang, and M. W. Wanlass, *Proceedings of the 38th IEEE Photovoltaics Specialists Conference* (Austin, TX, 2012), p. 1624.
3. Y. Chen, S. Farrell, G. Brill, P. Wijewarnasuriya, and N. Dhar, *J. Cryst. Growth* 310, 5303 (2008).
4. Z.C. Feng, A. Mascarenhas, and W.J. Choyke, *J. Lumin.* 35, 329 (1986).
5. C.B. Davis, D.D. Allred, and A. Reyes-Mena, *Phys. Rev. B* 47, 13363 (1993).

6. C.R. Corwine, J.R. Sites, T.A. Gessert, W.K. Metzger, P. Dippo, J. Li, A. Duda, and G. Teeter, *Appl. Phys. Lett.* 86, 221909 (2005).
7. T.H. Gfroerer, Y. Zhang, and M.W. Wanlass, *Appl. Phys. Lett.* 102, 012114 (2013).
8. F. Chen, Y. Zhang, T.H. Gfroerer, A.N. Finger, and M.W. Wanlass, *Proceedings of the 39th IEEE Photovoltaics Specialists Conference* (Tampa, FL, 2013), to be published.
9. N.C. GilesTaylor, R.N. Bicknell, D.K. Blanks, T.H. Myers, and J.F. Schetzina, *J. Vac. Sci. Technol. A* 3, 76 (1985).
10. W.J. Everson, C.K. Ard, J.L. Sepich, B.E. Dean, G.T. Neugebauer, and H.F. Schaake, *J. Electron. Mater.* 24, 505 (1995).